Green synthesis of silver nanoparticles using *Cordia dichotoma* leaves and their application as a corrosion inhibitor of mild steel in 1.0 M HCl

R.Q. Ibrahim,[1] S.H. Ali,[2] N.H. Faisal,[1] S.Q. Ibrahim,[3] A.A.A. Al-Shawi,[1]* A.N. Hassan,[1] M.Y. Kadhum[1]* and A.S. AbdulNabi[1]

[1]Department of Chemistry, College of Education for Pure Sciences, University of Basrah, Basrah, 61001, Iraq
[2]Department of Chemical and Petroleum Refining Engineering, College of Oil and Gas Engineering, Basrah University for Oil and Gas, Basrah, 61001, Iraq
[3]Department of Polymer and Petrochemical Engineering, College of Oil and Gas Engineering, Basrah University for Oil and Gas, Basrah, 61001, Iraq
**E-mail: ali.abdulhussein@uobasrah.edu.iq; mouayed.kadhum@uobasrah.edu.iq*

Abstract

In this study, a *Cordia dichotoma* plant extract was used to create silver nanoparticles (AgNPs), which were then analyzed using FT-IR, XRD, and SEM. To assess the AgNPs capacity to suppress corrosion, they were applied to mild steel at different concentrations (100–400 ppm) at temperatures of 298 K and 308 K in a corrosive medium containing 1.0 M hydrochloric acid. The corrosion-protective properties of AgNPs were investigated utilizing electrochemical impedance spectroscopy (EIS) and potentiodynamic polarization (PDP). The produced AgNPs showed an inhibitory efficiency of 94.93% in PDP and 87.33% in EIS at a concentration of 400 ppm. AgNPs function as a mixed-type inhibitor, which means that the inhibitor influences both the anodic and cathodic reactions, according to potentiodynamic polarization data. Additionally, the Langmuir adsorption isotherm was used to describe the adsorption behavior of the inhibitor. The estimated energy of adsorption ΔG_{ads} (−25.17 kJ/mol, −24.98 kJ/mol) indicates mixed physisorption and chemisorption interaction. These results suggest that the produced AgNPs have a great deal of potential as agents that limit corrosion. This study is revolutionary because it creates a green and sustainable nano-inhibitor that provides strong protection for mild steel surfaces and an environmentally friendly alternative to traditional inhibitors for possible industrial uses.

Received: February 12, 2026 Published: May 21, 2026 doi: 10.17675/2305-6894-2026-15-2-15

Keywords: *silver nanoparticles, green synthesis, corrosion inhibition, mild steel, electrochemical impedance spectroscopy, potentiodynamic polarization.*

Introduction

Metal surfaces deteriorate due to oxidation and reduction reactions, a common phenomenon known as corrosion [1]. The composition of the metal, its interactions with oxygen and acids, impurities, temperature, pH level, salt content, and humidity are the most significant factors that contribute to corrosion [2, 3]. Anodic and cathodic protection, protective coatings, and corrosion inhibitors are used to slow down or stop the rusting process. Chemicals known as corrosion inhibitors slow down or halt metal corrosion processes under corrosive conditions at small concentrations. Rust inhibitors are widely used because they are more effective and less expensive than alternative techniques [4–6]. Inhibitors work by forming a thin protective layer on a material's surface. This prevents dissolved oxygen from functioning or slows down any redox activities in corrosion systems [7, 8]. Conventional corrosion inhibitors are not appealing because they are toxic, expensive, difficult to prepare, and hazardous. Plant extracts, expired medications, plastic waste, surfactants, and nanomaterials are subjects of scientific studies that concentrate on the application of environmentally friendly corrosion inhibitors [9–13].

By adsorbing on the surface of iron or steel, these substances act as inhibitors [14]. The small size and large surface area to volume ratio of nanoparticles make them important materials [15]. Nanoparticles have been produced in a variety of ways depending on their intended use. Numerous studies have demonstrated that due to their higher surface-to-volume ratio compared to typical macroscale materials, they are good for preventing rust [16]. Businesses, industry, and the environment all greatly benefit from nanoparticles that prevent corrosion [17]. Since they prevent corrosive substances from penetrating the substrate surface, nanoparticles are useful for reinforcing materials [18]. Nanomaterials are the best inhibitors, but they become considerably more potent when compounds from plant extracts are added. Compared to hazardous organic inhibitors, plants and their extracts are inexpensive, harmless, and biodegradable [19].

Corrosion can be prevented by using extracts derived from various widely utilized plant parts, such as pulp, leaves, bark, roots, seeds, and peels. When these materials are present, the heteroatoms and π-electrons contained in their constituents provide adsorption on the surface, preventing metals and alloys from rusting [20, 21]. In warmer climates, *Cordia dichotoma* plants, such as shrubs and trees, are frequently found and have been used to treat diseases. Phenols, alkaloids, pyrrolizidine, triterpenoids, coumarins, and bioactive compounds are among the many phyto-constituents found in *Cordia dichotoma*. Corrosion inhibitors have been made from its seeds, leaves, and trunks [22]. Silver nanoparticles made from plant extracts are safe for the environment, need less energy, and can be produced on a big scale. Silver nanoparticles can prevent corrosion by applying a protective layer on metal surfaces [23].

AgNPs from cashew leaves have the capacity to prevent rust without damaging mild steel, as demonstrated by Ezzat *et al.* Rusting was investigated in saltwater simulations using electrochemical impedance spectroscopy and potentiodynamic polarization [24]. Tikoua

extract combined with nanomaterials shields steel from acidic conditions, according to the research by Farouq *et al.* When plant extract was combined with 100 ppm of ZnO nanomaterial, the greatest inhibitory impact was observed [25]. *Brassaiopsis hainla* extract was used by Budhathoki *et al.* to create nanoparticles that showed strong antibacterial activity and prevented acid-induced corrosion [26].

The ability of silver nanoparticles made from tobacco leaf extract to prevent carbon steel used in the petroleum industry from corroding when exposed to 1.0 M HCl was examined in a study by Al-Mhyawi *et al.* The maximum inhibition effectiveness of 98% was achieved by using 200 ppm of nanoparticles. When compared to other materials like ZnO, prior research has shown that AgNPs produced using green synthesis techniques are environmentally safe, provide superior surface coating, and have a high inhibitory efficiency. This illustrated the importance of AgNPs and their superior performance as a more potent and long-lasting corrosion inhibitor [27].

In this work, we synthesized and characterized silver nanoparticles (AgNPs) from *Cordia dichotoma* plant leaf extract. Temperature impacts and adsorption isotherms were investigated to establish the mechanism of corrosion inhibition. We examined mild steel from rusting in 1.0 M HCl using Electrochemical Impedance Spectroscopy and Potentiodynamic Polarization. The creation of an ecologically friendly and sustainable nano-inhibitor that offers strong protection for mild steel surfaces in contrast to conventional inhibitors for potential industrial uses is what sets this study apart.

Experimental section

Materials

Silver nitrate ($AgNO_3$) was purchased from Merck (Germany). Analytical grade hydrochloric acid was used to create a corrosive 1.0 M solution. Distilled water was used as a solvent in every experiment.

Preparation of plant extracts

Cordia dichotoma leaves are thoroughly washed, allowed to dry at room temperature for three days, and then chopped into tiny pieces to prepare them for the extraction process. A beaker containing 8 g of crushed leaves and 100 mL of distilled water is heated to 90°C for 30 min. To remove the dense material, the liquid was centrifuged after passing through filter paper. To ensure that the reducing and stabilizing agents had the greatest possible impact, the generated plant extract was used immediately for the creation of green nanoparticles.

Synthesis of silver nanoparticles

50 mL of 0.01 M silver nitrate and 6 ml of the plant extract (added dropwise) were stirred in a beaker for 15 min using a magnetic stirrer. The temperature was maintained between 45 and 50°C. The synthesis was carried out without any external adjustment at the pH of the

plant extract. The creation of AgNPs was indicated by the solution turning brown, which was subsequently separated by centrifuging it for 30 min at 4,000 rpm. The final pellet was meticulously cleaned with deionized water to make sure no residues remained. Lastly, the product was allowed to air dry at room temperature until it was completely dry [28].

Fourier Transform Infrared Spectroscopy (FT-IR)

AgNPs' functional groups and chemical bonds were identified by FT-IR spectroscopy. Pellets were made from KBr and mixed AgNPs using a hydraulic press. A Shimadzu 8400S Japan FT-IR spectrometer was used to record the spectra in the 400–4000 cm^{-1} range.

X-Ray Diffraction (XRD)

The XRD spectrum of AgNPs was recorded in the 2θ range of 10–80° using CuK_α radiation ($\lambda = 1.5406$) on a Philips X'Pert Pro diffractometer (PANalytical, Netherlands). The crystallite size (*D*) was calculated by Equation 1 (Scherrer's equation):

$$D = \frac{0.9\lambda}{\beta \cos\theta} \quad (1)$$

where λ is the radiation wavelength, β is the full width at half maximum of the diffraction peak, and θ is the Braggs angle.

Scanning Electron Microscopy (SEM)

A TESCAN MIRA3 field-emission scanning electron microscope was used to examine a modest amount of AgNPs on carbon-coated copper. The SEM uses a concentrated stream of electrons to survey the AgNPs surface. High-resolution images of the surface are produced by the electrons' interaction with the material, which produces secondary and scattering electrons. SEM pictures were acquired at different magnifications. An energy dispersive-equipped SEM was used to assess EDX analyses.

Corrosion inhibition experiment

50 mL of 1.0 M HCl was utilized as the corrosive blank solution. A tiny hole was made in mild steel, which was then exposed to varying concentrations of AgNPs (100, 200, 300, and 400 ppm) in 50 mL of 1.0 M HCl at temperatures between 298 K and 308 K. Mild steel was used as the working electrode in this study. The chemical composition of the mild steel is 99.16 Fe, 0.15 C, 0.40 Mn, 0.17 Si, 0.05 P, and 0.005 Al.

Electrochemical measurements

The electrochemical measurements (PDP and EIS) were performed on mild steel with a surface area of 1 cm^2 using a Vertex. One potentiostat/galvanostat and the corresponding software. The exposed surface was first polished with silicon carbide sandpaper. Acetone was used to degrease the surface, which was then cleaned twice with distilled water. Before

immersion in the corrosion media, the samples were allowed to dry at ambient temperature, both with and without AgNPs in 1.0 M HCl. A typical three-electrode electrochemical corrosion cell was used to perform PDP. Mild steel was used as the working electrode. Its potential was measured against the reference electrode. A saturated calomel (Hg/Hg_2Cl_2 saturated KCl) reference electrode was employed, while the auxiliary electrode was platinum. The cell was constructed of Pyrex glass and had a 250 mL capacity. The cell features internal and external sections designed for electrodes immersion and the solution containment. Before performing PDP electrochemical tests in the potential range of (±200) mV at a scan rate of 1.0 mV/s, the working electrode was immersed in the corrosive solution for 15 min to stabilize the open circuit potential (E_{ocp}). The EIS experiments were conducted at room temperature at the open circuit potential in the frequency range of 100 kHz to 10 mHz at an amplitude of 5 mV. All the electrochemical tests were conducted in triplicate under the same experimental conditions to confirm the accuracy of the results, and the values provided are the mean of three separate measurements. The corrosion rate and inhibition efficiency (%*IE*) can be calculated from the corrosion current values. The surface coverage (θ) and inhibition efficiency (%*IE*) were calculated using Equations 2 (which is based on the simplistic assumption that the corrosion inhibitor under study has a primarily blocking mechanism of action) and 3 [29]:

$$\theta = \frac{i^0 - i}{i^0} \tag{2}$$

$$\%IE = \frac{i^0 - i}{i^0} \cdot 100 \tag{3}$$

where i and i^0 are the corrosion current densities in the presence and absence of the inhibitor, respectively. The value of inhibition efficiency (%*IE*) was also calculated from EIS data using Equation 4 [12]:

$$\%IE = \frac{R_{ct} - R_{ct}^0}{R_{ct}} \tag{4}$$

where R_{ct} and R_{ct}^0 are the charge transfer resistance in the presence and absence of the inhibitor, respectively.

Results and Discussion

FTIR spectrum

Finding the functionally active sites in *Cordia dichotoma* leaf extract and determining the proper functional groups for silver nanoparticles can be done efficiently and affordably with FT-IR spectroscopy. Peaks at frequencies of 1029, 1369, 1510, 1647, 2935, and 3421 cm^{-1} are displayed in Figure 1.

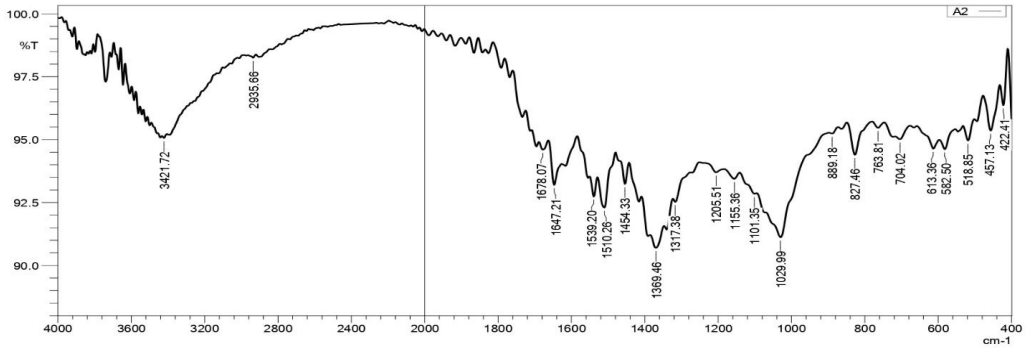

Figure 1. FT-IR spectrum of silver nanoparticles (AgNPs).

XRD analysis

XRD is one of the most important techniques for examining a variety of crystalline, powder, and amorphous materials. XRD can be used to measure particle size and describe different nanomaterials and their characteristics. Figure 2 shows that the diffraction peaks for the AgNPs at 2θ values of 23.56°, 27.80°, 32.24°, 38.05° and 46.24°. The obtained XRD pattern is consistent with a face-centered cubic silver structure, as confirmed by comparison with standard silver nanoparticle diffraction data. The fundamental peak for the creation of silver nanoparticles, the (111) plane of JCPDS card (04-0783) cubic silver, is represented by the observed diffraction peak at 38.05°. This phase is explained by the presence of naturally occurring chloride ions in the chemical components of the plant extract, which reacted with silver ions during the preparation process, in addition to the peaks at 27.80°, 32.24°, and 46.24°, which correspond to the crystalline levels (111), (200), and (220) of the silver chloride compound with the cubic crystal system according to JCPDS card (31-1238). This was supported by the EDX data, which showed a chlorine content of 2.64 wt.%. This resulted in the creation of a hybrid nanocomposite of silver and silver chloride, which improves the stability and catalytic activity of the nanoparticles. On the other hand, chemical substances from the plant extract or biomolecules surrounding the nanoparticles could be responsible for the peak at 23.56°. These findings show that the silver nanoparticles are hybrid crystalline.

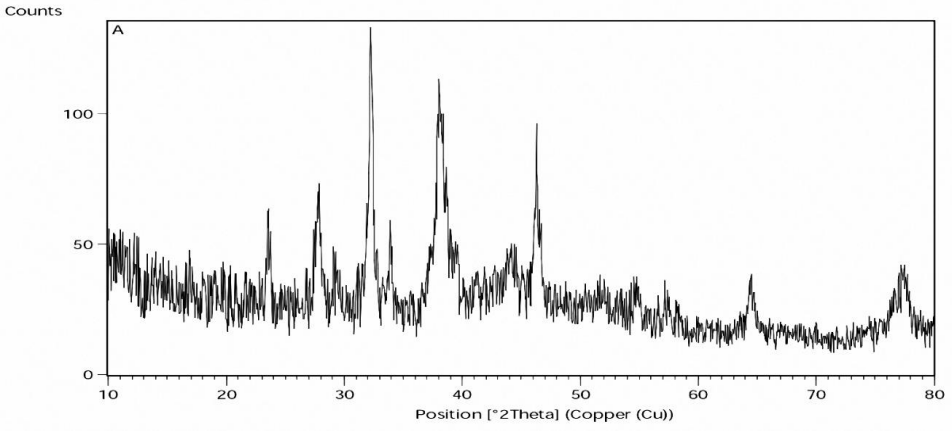

Figure 2. XRD spectrum of AgNPs showing five diffraction peaks 1–5.

As indicated in Table 1, the Scherrer equation (Equation 1) was used to determine the crystallite size (*D*) of the five peaks. The five computed *D* values are nearly identical. In comparison to the silver chloride phases, the metallic silver phase has the smallest crystallite size (17.01 nm) according to the computed crystal size values. This suggests that the plant extract's active components have a strong capacity to regulate silver crystal formation and stabilize them at the nanoscale. The growth of silver nanoparticle AgNPs crystallites is confirmed by the XRD data [30, 31].

Table 1. XRD data of AgNPs.

Peak No.	2θ	FWHM	Crystallite size (*D* nm)	Rel. Int%
1	23.5620	0.2952	27.43	30.50
2	27.8033	0.3936	20.75	39.97
3	32.2489	0.2952	27.93	100
4	38.055	0.4920	17.01	74.92
5	46.2412	0.3936	21.88	45.00

SEM analysis

SEM is used to show the surface morphology of nanoparticles, including their size, shape, distribution, and nanomaterial structure [32]. AgNPs made from *Cordia dichotoma* were examined using SEM. The findings showed that the AgNPs were agglomerated, spherical, and closely packed (Figure 3). Our findings are similar to those of Swapna G and Rao BK, who showed that the majority of the silver nanoparticles produced from *Cordia dichotoma* were spherical in shape [33]. The size of the nanoparticles was estimated because some of them were measured, and Figure 3 illustrates that they ranged from 150.68 to 234.17 nm. This suggests that there is some agglomeration among the tiny particles that are generated.

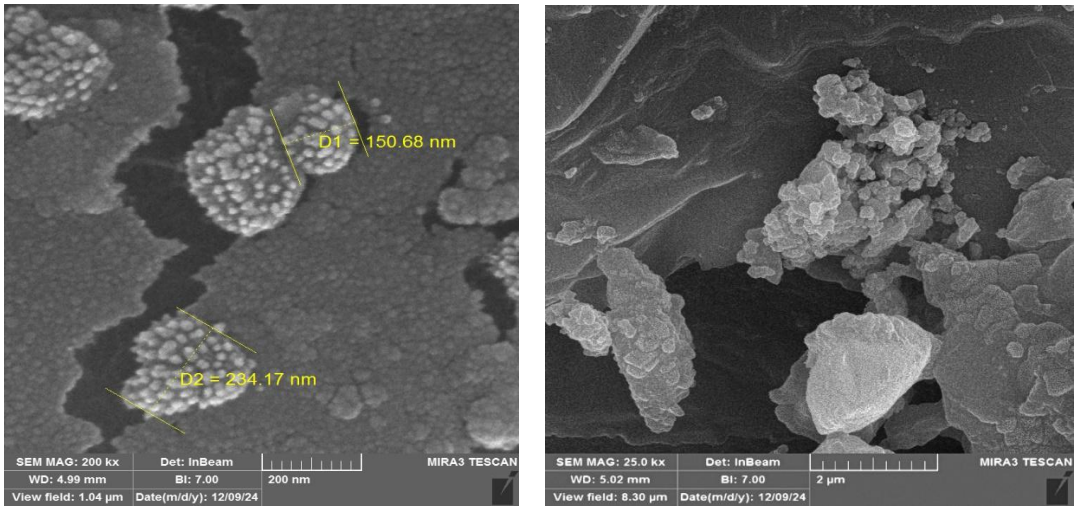

Figure 3. SEM images of AgNPs.

In order to provide interpretations of the elemental composition of the nanoparticle, SEM-EDX identifies the elements present and establishes their relative abundances [34]. The presence of elemental silver in the AgNPs was indicated by a significant peak in the EDX spectra at about 3.01 keV. The EDX of AgNPs [35, 36] reveals the presence of (in wt.%): C 0.29, O 0.53, Cl 2.64, Mg 1.26, and K 3.34.

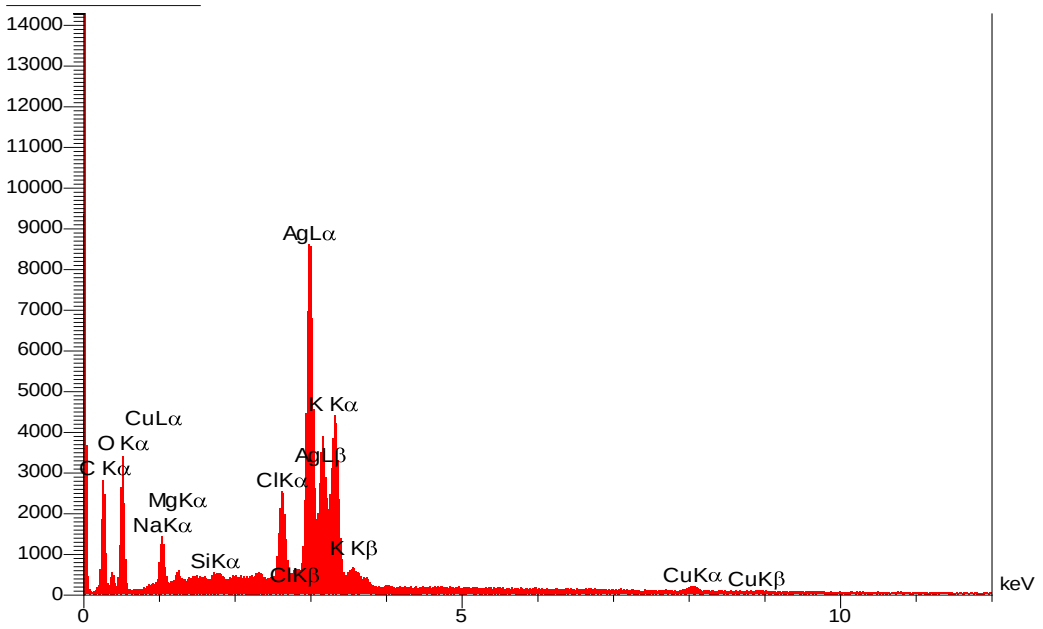

Figure 4. EDX analysis of AgNPs.

Potentiodynamic polarization measurements PDP

Figures 5 and 6 show the PDP curves for mild steel in 1.0M HCl with and without varying concentrations of AgNPs. Anodic and cathodic processes are significantly impacted by AgNPs inhibitors. They slow down the release of hydrogen during the cathodic process and the disintegration of metals during the anodic process. By extending the cathodic and anodic Tafel curves, we discovered that the corrosion current density (i_{corr}) and corrosion potential (E_{corr}) follow a straight line. Furthermore, increasing the concentration of *Cordia dichotoma* AgNPs (100–400 ppm) increased the surface coverage while decreasing the current density and corrosion rate [24]. The kind of inhibitor (anodic, cathodic, or mixed) is determined by comparing the corrosion potentials (E_{corr}) in the presence and absence of the inhibitor. If the difference (ΔE_{corr}) exceeds 80 mV, it indicates that the inhibitor is either cathodic or anodic. The observed changes indicate that the inhibitor is of mixed type because ΔE_{corr} is less than 80 mV. The E_{corr} readings in Table 2 primarily displayed the difference value. This indicates that E_{corr} value is not directional. Both anodic and cathodic reactions are impacted by the inhibitor, as seen by the observed fluctuations in E_{corr} values, both rising and falling. For example, the shift was cathodic at 100 ppm and anodic in relation to blank at 200 ppm. Consequently, the inhibitor is categorized as a mixed-type inhibitor [37].

Effect of inhibitor concentration

Table 2 displays the corrosion rate, the surface coverage (θ), and the inhibition efficiency (%*IE*) for mild steel in 1.0 M HCl at 298 K and 318 K, with or without AgNPs. The silver nanoparticle concentrations were 100, 200, 300, and 400 parts per million. The weight, corrosion rate, current density, and inhibition efficiency all decreased as the amount of AgNPs inhibitor increased. By forming a thin, passive protective layer on the steel surface and preventing electrochemical reactions, the AgNPs inhibitor slows down the corrosion process. This demonstrates that in acidic environments, silver nanoparticles (AgNPs) prevented the metal from corrosion [38, 39]. Table 2 demonstrates that as AgNPs concentrations rise, corrosion rates decrease and inhibition efficiency rises. The highest inhibitory efficiency was 94.93% at 298 K with 400 ppm of AgNPs, while the lowest was 66.37% at 308 K with 100 ppm.

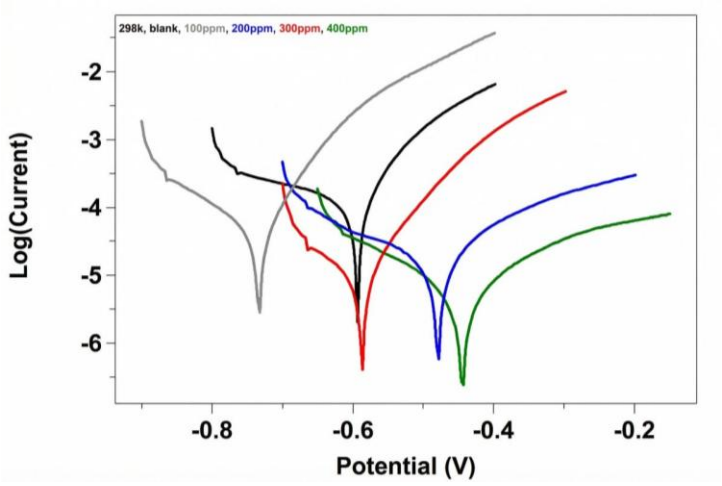

Figure 5. Potentiodynamic polarization corves for mild steel in 1.0 M HCl, in the presence and absence of different amounts of AgNPs, at 298 K.

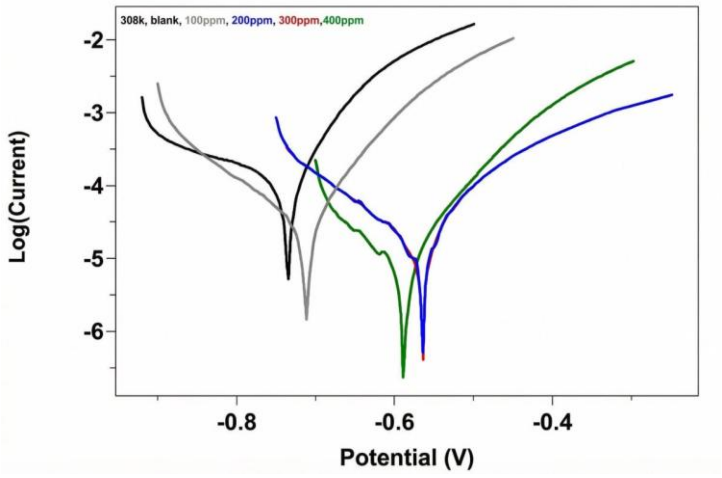

Figure 6. Potentiodynamic polarization corves for mild steel in 1.0 M HCl, in the presence and absence of different amounts of AgNPs, at 308 K.

Effect of temperature

The protective coating produced by these compounds on the steel surface is less effective at higher temperatures: %*IE* decreases with temperature, as shown in Table 2. Metals can be exposed to corrosive environments at higher temperatures, which could cause adsorbed molecules to desorb from the steel surface [40].

Table 2. Potentiodynamic polarization data for mild steel in 1.0 M HCl with and without different concentrations of AgNPs at 298 K and 308 K.

Concentration	T, K	E_{corr}, mV	i_{corr}, mA/cm^2	θ	Inhibition efficiency, %*IE*
Blank	298	590.2	0.11410	–	–
	308	734.2	0.15130	–	–
100 ppm	298	723.7	0.03837	0.736	73.66
	308	750.7	0.03984	0.663	66.37
200 ppm	298	470.4	0.01587	0.860	86.09
	308	564.8	0.02300	0.847	84.79
300 ppm	298	596.5	0.00784	0.931	93.12
	308	585.6	0.01979	0.869	86.92
400 ppm	298	440.2	0.00578	0.949	94.93
	308	586.7	0.01072	0.929	92.91

Electrochemical Impedance Spectroscopy (EIS)

The ability of the AgNPs to prevent corrosion was examined using the EIS approach. Impedance tests evaluate surface resistance, capacitance, corrosion inhibition, and characteristics of the mechanism that prevents corrosion. Nyquist and Bode plots for mild steel in 1.0 M HCl with and without varying concentrations of AgNPs are displayed in Figure 7. The real and imaginary parts of the impedance were plotted on the X and Y-axis, respectively. A Nyquist plot is created, and the center of the clearly depressed semicircle form in Figure 7a is below the real axis. As the inhibitor concentration increases, the semicircle becomes larger. The steel surface is protected by a stable adsorbed layer of the inhibitor active components, which functions as a barrier against the corrosive medium. The Bode plot in Figure 7b has two graphs, the frequency on the horizontal axis and the precise impedance (Z) values on the vertical axis are displayed in the first plot. The second plot displays the phase angle on the vertical axis and the frequency on the horizontal axis. Frequency and resistance are displayed on a logarithmic scale, whereas phase angle is typically displayed on a linear scale. By comparing the data to a straightforward equivalent circuit model in Figure 7c, the Nyquist plot impedance characteristics were confirmed.

Table 3 shows the double layer capacitance C_{dI}, charge transfer resistance R_{ct}, and solution resistance R_s.

The EIS results demonstrated that the tested system does not behave optimally, as evidenced by the gradual divergence in phase angle and inability to reach the ideal values, as well as the non-steep slope of impedance against frequency curves. The constant phase element (CPE) was employed since the behavior displayed above indicates that the inhibitory layer created on the metal surface is not entirely smooth and may have some rough areas or uneven molecule distribution. The value of *n*, which ranges from 0.83 to 0.89 as shown in Table 3, supports the non-ideal capacitive behavior of the electrochemical systems. Furthermore, the conformation quality was statistically assessed using (χ^2), a low chi-squared function, suggesting that the double layer features are reflected in the effective capacitance (C_{dI}) [40].

Table 3. The EIS results for mild steel in 1.0 M HCl in the presence and in the absence of different amounts of AgNPs at 298 K.

Concentration	R_s, **Ohm·cm²**	R_{ct}, **Ohm·cm²**	***n***	C_{dl}, **μF/cm²**	**Inhibition Efficiency, %*IE***	χ^2
Blank	0.271	11.36	0.83	140.101	–	$1.12\cdot10^{-3}$
100 ppm	0.283	77.21	0.85	20.613	85.28	$8.99\cdot10^{-4}$
200 ppm	0.286	80.51	0.86	19.768	85.88	$8.03\cdot10^{-4}$
300 ppm	0.291	87.16	0.87	18.260	86.96	$6.94\cdot10^{-4}$
400 ppm	0.312	89.67	0.89	17.749	87.33	$5.65\cdot10^{-4}$

This is an undesirable behavior that frequently occurs in real systems and indicates that the inhibitor is not functioning properly. However, the charge transfer resistance increased significantly in comparison to the blank when the inhibitor was added. This demonstrates the formation of a strong protective layer that reduces the corrosion rate [41, 42]. R_{ct} most likely increases along with the number of inhibitor molecules. This is either a result of the inhibitor molecules adhering to the electrode surface or an improvement in the properties and stability of the adsorbed protective film on the mild steel [43]. Table 3 demonstrates that the inhibition efficiency (%*IE*) and charge transfer resistance (R_{ct}) increased with the addition of more AgNPs inhibitor. This could be the result of the mild steel being covered for protection.

Conversely, the double layer capacitance C_{dI} decreases with an increase in inhibitor concentration. This decrease can result from a decrease in the local dielectric constant or from inhibitors adhering to the mild steel's surface and increasing the thickness of the protective layer [44]. Out of all the concentrations examined, Table 3 demonstrates that the concentration of 400 ppm had the highest inhibitory efficiency (%*IE*).

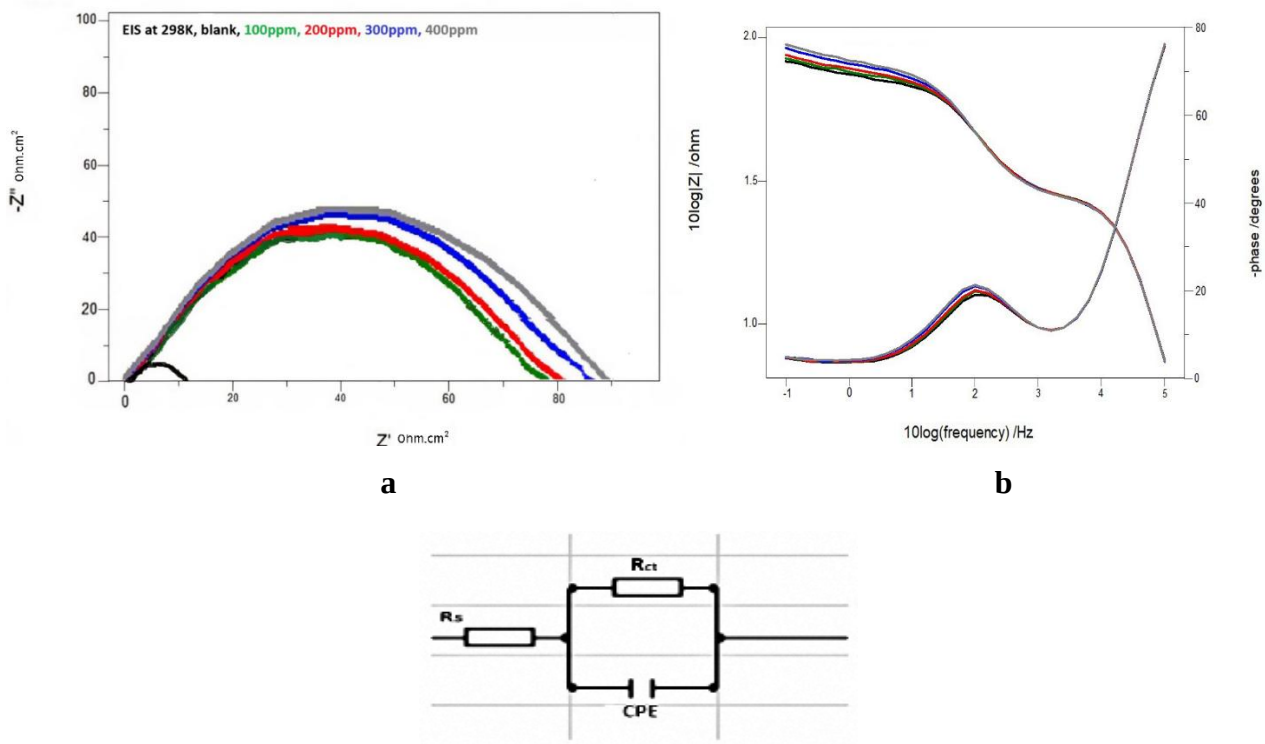

Figure 7. EIS measurement findings for mild steel in 1.0 M HCl with and without different concentrations of AgNPs at 298 K, **a –** Nyquist plot; **b –** Bode plot; **c –** equivalent circuit model.

Adsorption isotherm

Depending on the kind of adsorbent and adsorbate, the adsorption of inhibitors on metal surfaces contributes significantly to their inhibitory activity. The adsorption of the AgNPs inhibitor on mild steel surfaces was investigated using potentiodynamic polarization data. Plotting (C/θ) against the concentration of the AgNPs inhibitor (C) allowed for a visual analysis of the data. Using the Langmuir Equation 5 [45], adsorption isotherm analysis sheds light on the inhibitor's interaction with the metal surfaces.

$$\frac{C}{\theta} = \frac{1}{K_{ads}} + C \tag{5}$$

where C, θ and K_{ads} is the concentration of the AgNPs, surface coverage, and adsorption constant, respectively.

Figure 8 shows the K_{ads} values for the AgNPs, calculated based on the Langmuir adsorption isotherm for the inhibitor on the mild steel surface at two testing temperatures. The straight lines with slopes of 0.9516 and 0.9484 and R^2 values of 0.9994 and 0.9975, respectively, show a high correlation with the Langmuir adsorption model, which is very close to the theoretical value of unity and has an intercept of $1/K_{ads}$ [27]. Equation 6 [46, 47]

determines the relationship between the value of K_{ads} and the standard free energy of adsorption (ΔG_{ads}):

$$\Delta G_{ads} = -RT \ln(C_W K_{ads}) \quad (6)$$

where R is the universal gas constant, T is the absolute temperature, C_w is the concentration of water molecules in the solution in mg/L, and K_{ads} is the adsorption constant.

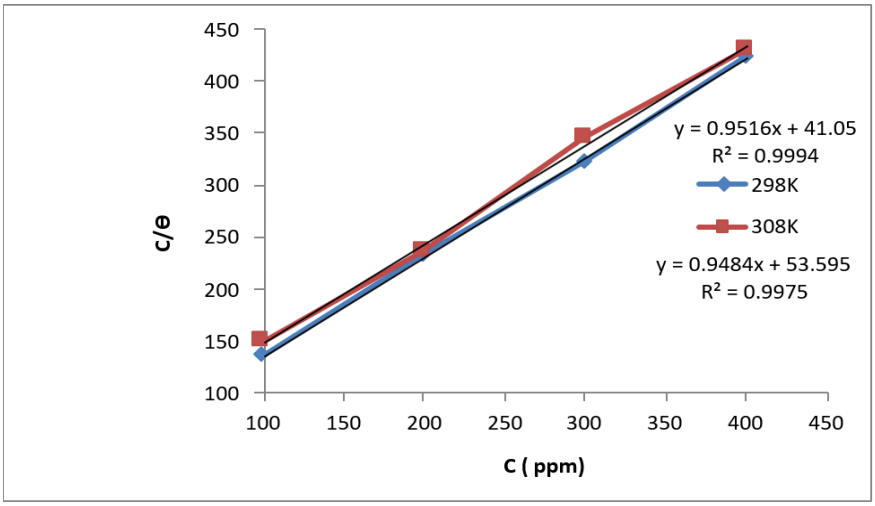

Figure 8. Langmuir adsorption isotherm for mild steel in 1.0 M HCl with different amounts of AgNPs at temperatures of 298 K and 318 K.

When the G_{ads} levels are less than –20 kJ/mol, physical adsorption takes place; when ΔG_{ads} values are more than –40 kJ/mol, chemical adsorption takes place. The results of the investigation indicate mixed adsorption processes involving both physisorption and chemisorption interaction, with ΔG_{ads} being –25.17 kJ/mol at 308 K and –24.98 kJ/mol at 298 K. The AgNPs adhere to the metal surface spontaneously because ΔG_{ads} is negative [48, 49]. The results for the current inhibitor produced utilizing an environmentally friendly method were compared to those of other inhibitors reported in the literature under comparable experimental settings, as summarized in Table 4, in order to contextualize the research findings.

Table 4. Comparing the present AgNPs' inhibitory effectiveness to that of previously documented green inhibitors.

Inhibitor Type	Medium	Temp	Metal type	Inhibition Efficiency %*IE*	Ref.
AgNPs of *cordia dichotoma* extract	1.0 M HCl	298 K	Mild steel	94.93 PDP at 400 ppm 87.33 EIS at 400 ppm	Current study
		303 K		92.91 PDP at 400 ppm	
AgNPs of *tobacco* leaf extract	1.0 M HCl	303 K	Carbon steel	95.3 PDP at 200 ppm 93.2 EIS at 200 ppm	27

Inhibitor Type	Medium	Temp	Metal type	Inhibition Efficiency %*IE*	Ref.
AgNPs of *kolanut pod* extract	1.0 M HCl	298 K	Mild steel	99.59 PDP at 20 µg/ml	23
Cryptocarya nigra extract	1.0 M HCl	303 K	Mild steel	82.64 PDP at 500 ppm 91.05 EIS at 500 ppm	1
Spinacia oleracea extract	1.0 M HCl	303 K	Carbon steel	91.1 PDP at 500 ppm 92.4 EIS at 500 ppm	39

When comparing the results in the above table, one can see that while the inhibitory efficiency of the raw plant extracts is good, while employing AgNPs made from plant extracts significantly improves the inhibition efficiency. The enormous surface area of the nanoparticles and their capacity to stick to the metal surface are responsible for this enhancement. The type of functional groups in the plant extract and the size of the nanoparticles may be the reason why certain studies have reached maximal efficiency, even if the results in this study are consistent with previous eco-friendly nano-inhibitors. However, compared to conventional industrial inhibitors, which can be hazardous and seriously pollute the environment, the AgNPs produced in this study provide an affordable, eco-friendly, and efficient substitute. In addition to protecting steel against corrosion during metal cleaning and rust removal using potent acidic solutions, they can be employed as corrosion inhibitors to safeguard oil pipelines and subterranean equipment. This approach maintains the metal's mechanical properties, integrity, and efficiency required for use in a range of industrial applications.

Conclusions

The production of AgNPs was investigated using FT-IR, XRD, SEM, and EDX. In a 1.0 M HCl environment, *Cordia dichotoma* AgNPs successfully prevent mild steel from corroding. More precise assessments of mild steel corrosion and inhibitor effectiveness can be obtained by electrochemical methods. AgNPs function as a mixed inhibitor, according to PDP curves for mild steel in 1.0 M HCl. The inhibition efficiency (%*IE*) increases with increasing AgNP concentration and decreases with increasing temperature. According to the EIS data, the semicircle size in the Nyquist plots increases with the inhibitor content, the double layer capacitance decreases, while the inhibition efficiency and charge transfer resistance increase. According to the results of characterization and electrochemical studies, the AgNPs based on *Cordia dichotoma* show promise as an inhibitor for corrosion prevention.

Funding

Self-funded by authors.

Availability of data and material

The datasets used and analyzed during the current study are available from the corresponding author on reasonable request.

Conflict of interests

The authors declare that they have no competing interests.

Acknowledgements

This research project is supported by the Department of Chemistry, College of Education for Pure Sciences, University of Basrah, Basrah, Iraq **Contribution statement AAA** and **RQI** contributed to designing, analysis, and writing the manuscript; **NHF, SHA, SQI, ANH, MYK,** and **ASA** contributed to the synthesis and analysis experiments. All authors approved the final version of the manuscript.

References

1. M. Faiz, A. Zahari, K. Awang, and H. Hussin, Corrosion inhibition on mild steel in 1 M HCl solution by Cryptocarya nigra extracts and three of its constituents (alkaloids), *RSC Adv*., 2020, **10**, no. 11, 6547–6562. doi: 10.1039/c9ra05654h
2. R.S.A. Hameed, Schiff'bases as corrosion inhibitor for aluminum alloy in hydrochloric acid medium, *Tenside, Surfactants, Deterg*., 2019, **56**, no. 3, 209–215. doi: 10.3139/113.110622
3. M.M. Hanoon, A.M. Resen, L.M. Shaker, A.A.H. Kadhum and A.A. Al-Amiery, Corrosion investigation of mild steel in aqueous hydrochloric acid environment using n-(Naphthalen-1yl)-1-(4-pyridinyl) methanimine complemented with antibacterial studies, *Biointerface Res. Appl. Chem*., 2021, **11**, no. 2, 9735–9743. doi: 10.33263/BRIAC112.97359743
4. A.M. Resen, M. Hanoon, R.D. Salim, A.A. Al-Amiery, L.M. Shaker and A.A. Kadhum, Gravimetrical, theoretical, and surface morphological investigations of corrosion inhibition effect of 4-(benzoimidazole-2-yl) pyridine on mild steel in hydrochloric acid, *Koroz. ochr. mater*., 2020, **64**, no. 4, 122–130. doi: 10.2478/kom-2020-0018
5. A.J. Eltmimi, A. Alamiery, A.J. Allami, R.M. Yusop, A.H. Kadhum and T. Allami, Inhibitive effects of a novel efficient Schiff base on mild steel in hydrochloric acid environment, *Int. J. Corros. Scale. Inhib*., 2021, **10**, no. 2, 634–648. doi: 10.17675/2305-6894-2021-10-2-10
6. J.K. Odusote, T.B. Asafa, J.G. Oseni, A.A. Adeleke, A.A. Adediran, R.A. Yahya, J.M. Abdul and S.A. Adedayo, Inhibition efficiency of gold nanoparticles on corrosion of mild steel, stainless steel and aluminium in 1 M HCl solution, *Mater. Today: Proc*., 2021, **38**, 578–583. doi: 10.1016/j.matpr.2020.02.984

7. A. Singh, E. Ebenso and M.A. Quraishi, Corrosion inhibition of carbon steel in HCl solution by some plant extracts, *Int. J. Corros*., 2012, **2012**, no. 1, 897430. doi: 10.1155/2012/897430
8. M.S. Rukaiyat, G.S. Abubakar and M.K. Fatima, Corrosion inhibition of mild steel using alkaloids and tannins extracts of Jatropha curcas in acidic media, *Bayero. J. Pure Appl. Sci*., 2017, **10**, no. 1, 311–317. doi: 10.4314/bajopas.v10i1.62S
9. R.M. Bandeira, F.P. Lima, M.S. Nunes, E.C. dos Santos, J.R. dos Santos Júnior, J.M.E. de Matos, C.M. Feitosa, M. Rai, S. Bhattarai and D.D. Mulmi, The green plant-based corrosion inhibitors-a sustainable strategy for corrosion protection, *Surf. Sci. Technol*., 2025, **3**, no. 1, 19. doi: 10.1007/s44251-025-00084-7
10. R.S.A. Hameed and A.M. Al-Bonayan, Recycling of some water soluble drugs for corrosion inhibition of steel materials: analytical and electrochemical measurements, *Journal of Optoelectronic and Biomedical Materials*, 2021, **13**, no. 2, 45–55. doi: 10.15251/JOBM.2021.132.45
11. A.H. Yasir, A.S. Khalaf and M.N. Khalaf, Preparation and characterization of oligomer from recycled PET and evaluated as a corrosion inhibitor for C-steel material in 0.1 M HCl, *Open J. Org. Polym. Mater*., 2017, **7**, 1–15. doi: 10.4236/ojopm.2017.71001
12. R.S.A. Hameed, Cationic surfactant-Zn^{+2} systems as mixed corrosion inhibitors for carbon steel in a sodium chloride corrosive medium, *Port. Electrochim. Acta*, 2018, **36**, no. 4, 271–283. doi: 10.4152/pea.201804271
13. M.A. Raheem, Z.A. Abdulnabi and A.A.A. Al-Shawi, Synthesis and characterization of multiwalled carbon nanotubes decorated by ZnO and Ag_2O for using to remove methyl green and Erythrosin B dyes from their aqueous solutions, *Annales de Chimie - Science des Matériaux*, 2025, **49**, no. 1, 83–93. doi: 10.18280/acsm.490111
14. A.S. Al-Gorair, H. Hawsawi, A. Fawzy, M. Sobhi, A. Alharbi, R.S.A. Hameed, S. Abd El Wanees and M. Abdallah, Evaluation of the anticorrosion and adsorption properties of polyethylene glycol and polyvinyl alcohol for corrosion of iron in 1.0 M NaCl solution, *Int. J. Electrochem. Sci*., 2021, **16**, no. 11, 211119. doi: 10.20964/2021.11.03
15. N.A.M. Obaid, N.H. Faisal, N.W. Ali, R.G. Ibrahim, A.N. Hassan, A.J. Kadhum, A.A.A. Al-Shawia, M.E. Mohmmed and M. Abdalla, Synthesis, characterization, and biological activity of silver nanofibers essential oils of prunus dulcis, *Egypt. Pharm. J*., 2025, **24**, no. 1, 58–68. doi: 10.4103/epj.epj_226_24
16. P. Jain, B. Patidar and J. Bhawsar, Potential of nanoparticles as a corrosion inhibitor: a review, *J. Bio Tribo Corros*., 2020, **6**, no. 2, 43. doi: 10.1007/s40735-020-00335-0
17. R.S.A. Hameed, S. Obeidat, M.T. Qureshi, S.R. Al-Mhyawi, E.H. Aljuhani and M. Abdallah, Silver nanoparticles–Expired medicinal drugs waste accumulated at hail city for the local manufacturing of green corrosion inhibitor system for steel in acidic environment, *J. Mater. Res. Technol*., 2022, **21**, 2743–2756. doi: 10.1016/j.jmrt.2022.10.081

18. R.A. Hameed, M. Faride, M. Othman, B. Huwaimel, S. Al-Mhyawi, A. Shamroukh, F. Alshammary, E. Aljuhan and M. Abdallah, Green synthesis of zinc sulfide nanoparticles-organic heterocyclic polyol system as eco-friendly anti corrosion and anti-bacterial corrosion inhibitor for steel in acidic environment, *Green Chem. Lett. Rev*., 2022, **15**, no. 3, 847–862. doi: 10.1080/17518253.2022.2141585
19. L.M. Muresan, Nanocomposite coatings for anti-corrosion properties of metallic substrates, *Materials*, 2023, **16**, no. 14, 5092. doi: 10.3390/ma16145092
20. N. Hossain, M.A. Islam and M.A. Chowdhury, Advances of plant-extracted inhibitors in metal corrosion reduction future prospects and challenges, *Results Chem*., 2023, **5**, 100883. doi: 10.1016/j.rechem.2023.100883
21. Z. Al-Abdullah, A.A. AL-Shawi, M.N. Aboud, B.A. Alabdulaziz, H. Al-Furaiji and I.N. Luaibi, Synthesis and Analytical Characterization of Gold Nanoparticles using Microwave-Assisted Extraction System and Study their Application in Degradation, *J. Nanostruct*., 2020, **10**, no. 4, 682–690.
22. V. Anisha and M. Kumar, A critical review on Cordia dichotoma: Its therapeutic value, *Pharma Innov. J*., 2022, **11**, no. 6, 668–677.
23. T.B. Asafa, J.K. Odusote, O.S. Ibrahim, A. Lateef, M.O. Durowoju, M.A. Azeez, T.A. Yekeen, I.C. Oladipo, E.A. Adebayo, J.A. Badmus, Y.K. Sanusi and O. Adedokun, Inhibition efficiency of silver nanoparticles solution on corrosion of mild steel, stainless steel and aluminum in 1.0 M HCl medium, *IOP Conf. Ser.:Mater. Sci. Eng*., **2020**, 012018. doi: 10.1088/1757-899X/805/1/012018
24. A.O. Ezzat, V.S. Aigbodion, H.A. Al-Lohedan and C.J. Ozoude, Unveiling the corrosion inhibition efficacy and stability of silver nanoparticles synthesized using Anacardium occidentale leaf extract for mild steel in a simulated seawater solution, *RSC Adv*., 2024, **14**, no. 26, 18395–18405. doi: 10.1039/d4ra02362e
25. R. Farouq, E. Hamdy, M.M.S. Abbassy and H.A. Farag, Utilizing nanomaterials to functionalize the Tikoua extract as a powerful green anti-corrosion inhibitor for carbon steel, *J. Pet. Explor. Prod. Technol*., 2025, **15**, no. 9, 143. doi: 10.1007/s13202-025-02060-1
26. S. Budhathoki, N. Chaudhary, B. Guragain, D. Baral, J. Adhikari and N.K. Chaudhary, Green synthesis of silver nanoparticles from Brassaiopsis hainla extract for the evaluation of antibacterial and anticorrosion properties, *Heliyon*, 2024**,** **10**, no. 15, e35642. doi: 10.1016/j.heliyon.2024.e35642
27. S.R. Al-Mhyawi, Green synthesis of silver nanoparticles and their inhibitory efficacy on corrosion of carbon steel in hydrochloric acid solution, *Int. J. Electrochem. Sci*., 2023, **18**, no. 9, 100210. doi: 10.1016/j.ijoes.2023.100210
28. M.J. Sultana, A.I.S. Nibir and F.R.S Ahmed, Biosensing and anti-inflammatory effects of silver, copper and iron nanoparticles from the leaf extract of Catharanthus roseus, *Beni-Suef Univ. J. Basic Appl. Sci*., 2023, **12**, 26. doi: 10.1186/s43088-023-00358-9

29. R. Abdel-Hameed, G.M.S. Aleid, H. Ragab, H. Alshafey and A.M. Alosaimi, Synthesis, characterization, and evaluation of polymeric surfactants derived from PET plastic waste as green corrosion inhibitor of steel surfaces in marine environment for heavy industry, *RSC Adv*., 2023, **13**, no. 45, 31969–31988. doi: 10.1039/d3ra04518h
30. W. Dagher, A. Alassod, M.F. Al Hinnawi, I. Alghoraibi, A. Taher and M. Alnhlaoui, Characterization and antibacterial effect of green-synthesised silver nanoparticles using different extraction methods from *Ziziphus spina-christi* (Sidr) leaf extract collected from Syria, *RSC Adv*., 2025, **15**, no. 42, 35642–35659. doi: 10.1039/d5ra05214a
31. N.H. Faisal, N.A.M. Obaid, N.W. Ali, A.A.A. Al-Shawi, R.G. Ibrahim, A.N. Hassan, A.J. Kadhum, O.A. Mohsein and I.N. Luaibi, Green Synthesis of Silver Nanoparticles Using the Seeds of Lupinus luteus: Characterization and Assessment the Antibacterial and Anticancer Activities, *Asian Pac. J. Cancer Prev*., 2025, **26**, no. 9, 3405–3414. doi: 10.31557/APJCP.2025.26.9.3405
32. N.S. Alharbi, N.S. Alsubhi and A.I. Felimban, Green synthesis of silver nanoparticles using medicinal plants: Characterization and application, *J. Radiat. Res. Appl. Sci*., 2022, **15**, no. 3, 109–124. doi: 10.1016/j.jrras.2022.06.012
33. G. Swapna and B.K. Rao, Green Synthesis and Characterization of Silver Nanoparticles from Stem Bark Extract of Cordia dichotoma G. Forst and Evaluation of their Antioxidant and Antibacterial activities, *Pharmacogn. Res*., 2021, **13**, no. 3, 158–164. doi: 10.5530/pres.13.3.8
34. N.C. Nkosi, A.K. Basson, Z.G. Ntombela, N.G. Dlamini and R.R. Pullabhotla, Green Synthesis, Characterization and Application of Silver Nanoparticles Using Bioflocculant: A Review, *Bioengineering*, 2024, **11**, no. 5, 492. doi: 10.3390/bioengineering11050492
35. M.A. Abd-Elraheem, M.A.A. Soliman, A.S. Bashandy, W. Abd-Elhamed, G.S. Alfawal and M.A. Elshaer, Efficiency Of Green Synthetic Silver And Iron Nanoparticles Of Acacia nilotica Pods Against Plant Pathogenic Bacteria And Land Snails, *Egypt. J. Soil. Sci*., 2024, **64**, no. 3, 1033–1052.
36. H.K. Thawini and A.A. Al-Shawi, A polysaccharide of Ziziphus spina-Christi L., and it's Silver nanoparticles induced reactive oxygen species and late apoptosis of Liver cancer cells, *Nanomedicine Res. J*., 2021, **6**, no. 3, 237–247. doi: 10.22034/NMRJ.2021.03.004
37. R. Abdel-Hameed, M.T. Qureshi, M. Abdallah, E. Aljuhani, A.A. Alzharani, A. Alfarsi, A.M. Bakry, B. Huwaimel and O. Farghaly, Recycling of expired lactulose drugs as eco-friendly corrosion inhibitor for steel alloys in acidic environment: gravimetrical and electrochemical studies, *Int. J. Electrochem. Sci*., 2022, **17**, no. 12, 221270. doi: 10.20964/2022.12.92
38. V.O. Egbeneje, S.E. Okhale, C. Imoisi, I.O. Ogbogo and O. Ojo, Evaluation of the inhibitive properties of silver nanoparticles in Senna occidentalis root extract as corrosion inhibitor of mild steel, *Tanzania J. Sci*., 2023, **49**, no. 3, 655–663. doi: 10.4314/tjs.v49i3.9

39. R.S.A. Hameed, G.M.S. Aleid, D. Mohammad, M.M. Badr, B. Huwaimel, M.Sh. Suliman, F. Alshammary and M. Abdallah, Spinacia oleracea extract as green corrosion inhibitor for carbon steel in hydrochloric acid solution, *Int. J. Electrochem. Sci*., 2022, **17**, no. 10, 221017. doi: 10.20964/2022.10.31
40. R.S. Hameed, Solvent Free Glycolysis of Plastic Waste as Green Corrosion Inhibitor for Carbon Steel in Sulfuric Acid, *J. New Mater. Electrochem. Syst*., 2017, **20**, no. 3, 141–149.
41. A.Y. Rubaye, A.A. Abdulwahid, S.B. Al-Baghdadi, A.A. Al-Amiery, A.A. Kadhum and A.B. Mohamad, Cheery sticks plant extract as a green corrosion inhibitor complemented with LC-EIS/MS spectroscopy, *Int. J. Electrochem. Sci*., 2015, **10**, no. 10, 8200–8209. doi: 10.1016/s1452-3981(23)11087-x
42. A.B. Mohamad, A.A. Kadhum, A.A. Al-Amiery, L.C. Ying and A.Y. Musa, Synergistic of a coumarin derivative with potassium iodide on the corrosion inhibition of aluminum alloy in 1.0 M H_2SO_4, *Met. Mater. Int*., 2014, **20**, 459–467. doi: 10.1007/s12540-014-3008-3
43. E.A. Şahin, R. Solmaz, İ.H. Gecibesler and G. Kardaş, Adsorption ability, stability and corrosion inhibition mechanism of phoenix dactylifera extrat on mild steel, *Mater. Res. Express*., 2020, **7**, no. 1, 016585. doi: 10.1088/2053-1591/ab6ad3
44. M. Belkhaouda, L. Bammou, R. Salghi, A. Zarrouk, E.E. Ebenso, H. Zarrok and B. Hammouti, Inedible avocado extract: an efficient inhibitor of carbon steel corrosion in hydrochloric acid, *Int. J. Electrochem. Sci*., 2013, **8**, no. 9, 10987−10999. doi: 10.1016/S1452-3981(23)13164-6
45. A. Kokalj, On the use of the Langmuir and other adsorption isotherms in corrosion inhibition. *Corros. Sci*., 2023, **217**, 111112. doi: 10.1016/j.corsci.2023.111112
46. R.S.A. Hameed, Ranitidine drugs as non-toxic corrosion inhibitors for mild steel in hydrochloric acid medium, *Port. Electrochim. Acta*., 2011, **29**, no. 4, 273–285.
47. M. Hrimla, A. Alahyane, A. Oubella, L. Bahsis, J. Ayour, I. Elateri, M. Abderrazik, H. Anane and M.R. Laamari, Inhibitive Properties of Date Seed Extracts (Phoenix Dactylifera L.) on Mild Steel Corrosion in 1M HCl Solution: Experimental and DFT Studies, *Biointerface Res. Appl. Chem.*, 2023, **13**, no. 5, 427. doi: 10.33263/BRIAC135.427
48. M. Pourmohseni, A. Rashidi and M. Karimkhani, Preparation of corrosion inhibitor from natural plant for mild stil immersed in an acidic environmental: experimental and theoretical study, *Sci. Rep*., 2024, **14**, no. 1, 7937. doi: 10.1038/s41598-024-58637-z
49. E. Ituen, A. Singh, L. Yuanhua and O. Akaranta, Green synthesis and anticorrosion effect of Allium cepa peels extract-silver nanoparticles composite in simulated oilfield pickling solution, *SN Appl. Sci*., 2021, **3**, no. 6, 679. doi: 10.1007/s42452-021-04670-w

♦ ♦ ♦